

Research article

## Modulation of L-type $\text{Ca}^{2+}$ current but not activation of $\text{Ca}^{2+}$ release by the $\gamma_1$ subunit of the dihydropyridine receptor of skeletal muscle

Chris A Ahern<sup>1,1</sup>, Patricia A Powers<sup>2</sup>, Gloria H Biddlecome<sup>3,4</sup>,  
 Laura Roethe<sup>2</sup>, Paola Vallejo<sup>1</sup>, Lindsay Mortenson<sup>1</sup>, Caroline Strube<sup>5</sup>,  
 Kevin P Campbell<sup>3,4</sup>, Roberto Coronado<sup>1</sup> and Ronald G Gregg<sup>\*6</sup>

Address: <sup>1</sup>Department of Physiology, University of Wisconsin School of Medicine, and, <sup>2</sup>Biotechnology Center, University of Wisconsin, Madison, WI, 53706, USA; <sup>3</sup>Howard Hughes Medical Institute, and, <sup>4</sup>Departments of Physiology and Biophysics, and Neurology, The University of Iowa College of Medicine, Iowa City, IA, 52242, USA; <sup>5</sup>Laboratoire de Physiologie des Elements Excitables, Universite Claude Bernard - Lyon 1, France; and <sup>6</sup>Department of Biochemistry and Molecular Biology, and Department of Ophthalmology and Visual Sciences, University of Louisville, Louisville, KY, 40202, USA

E-mail: Chris A Ahern - [cahern@physiology.wisc.edu](mailto:cahern@physiology.wisc.edu); Patricia A Powers - [papowers@facstaff.wisc.edu](mailto:papowers@facstaff.wisc.edu);  
 Gloria H Biddlecome - [gloriab@amgen.com](mailto:gloriab@amgen.com); Laura Roethe - [lroethe@facstaff.wisc.edu](mailto:lroethe@facstaff.wisc.edu); Paola Vallejo - [paolavallejo@hotmail.com](mailto:paolavallejo@hotmail.com);  
 Lindsay Mortenson - [lindsay@physiology.uiowa.edu](mailto:lindsay@physiology.uiowa.edu); Caroline Strube - [caroline.strube@univ-lyon1.fr](mailto:caroline.strube@univ-lyon1.fr);  
 Kevin P Campbell - [campbellk@physiology.uiowa.edu](mailto:campbellk@physiology.uiowa.edu); Roberto Coronado - [coronado@physiology.wisc.edu](mailto:coronado@physiology.wisc.edu);  
 Ronald G Gregg\* - [ron.gregg@louisville.edu](mailto:ron.gregg@louisville.edu)

\*Corresponding author

Published: 24 July 2001

Received: 23 April 2001

BMC Physiology 2001, 1:8

Accepted: 24 July 2001

This article is available from: <http://www.biomedcentral.com/1472-6793/1/8>

© 2001 Ahern et al; licensee BioMed Central Ltd. Verbatim copying and redistribution of this article are permitted in any medium for any non-commercial purpose, provided this notice is preserved along with the article's original URL. For commercial use, contact [info@biomedcentral.com](mailto:info@biomedcentral.com)

### Abstract

**Background:** The multisubunit ( $\alpha_{1S}$ ,  $\alpha_2$ - $\delta$ ,  $\beta_{1a}$  and  $\gamma_1$ ) skeletal muscle dihydropyridine receptor (DHPR) transduces membrane depolarization into release of  $\text{Ca}^{2+}$  from the sarcoplasmic reticulum (SR) and also acts as an L-type  $\text{Ca}^{2+}$  channel. To more fully investigate the function of the  $\gamma_1$  subunit in these two processes, we produced mice lacking this subunit by gene targeting.

**Results:** Mice lacking the DHPR  $\gamma_1$  subunit ( $\gamma_1$  null) survive to adulthood, are fertile and have no obvious gross phenotypic abnormalities. The  $\gamma_1$  subunit is expressed at approximately half the normal level in heterozygous mice ( $\gamma_1$  het). The density of the L-type  $\text{Ca}^{2+}$  current in  $\gamma_1$  null and  $\gamma_1$  het myotubes was higher than in controls. Inactivation of the  $\text{Ca}^{2+}$  current produced by a long depolarization was slower and incomplete in  $\gamma_1$  null and  $\gamma_1$  het myotubes, and was shifted to a more positive potential than in controls. However, the half-activation potential of intramembrane charge movements was not shifted, and the maximum density of the total charge was unchanged. Also, no shift was observed in the voltage-dependence of  $\text{Ca}^{2+}$  transients.  $\gamma_1$  null and  $\gamma_1$  het myotubes had the same peak  $\text{Ca}^{2+}$  amplitude vs. voltage relationship as control myotubes.

**Conclusions:** The L-type  $\text{Ca}^{2+}$  channel function, but not the SR  $\text{Ca}^{2+}$  release triggering function of the skeletal muscle dihydropyridine receptor, is modulated by the  $\gamma_1$  subunit.

### Background

In skeletal muscle, the dihydropyridine receptor (DHPR)

consists of  $\alpha_{1S}$ ,  $\alpha_2$ - $\delta$ ,  $\beta_{1a}$  and  $\gamma_1$  subunits [1]. This complex is responsible for the L-type  $\text{Ca}^{2+}$  current and serves as

the voltage sensor for excitation-contraction (EC) coupling. In the latter process, the movement of electrical charges in the  $\alpha_{1S}$  subunit promotes a conformational change that opens the ryanodine receptor type-1 (RyR1) in the sarcoplasmic reticulum membrane (SR) leading to an increase in cytosolic  $Ca^{2+}$  [2,3]. The functional interactions between the DHPR subunits necessary for opening the  $Ca^{2+}$  channel are only partially known. Further, the interactions between DHPR subunits and RyR1 also are incompletely understood. The  $\alpha_1$  subunit is a large protein that contains the basic functional elements of the L-type  $Ca^{2+}$  channel, including the  $Ca^{2+}$  selectivity, voltage-dependent gating, and sensitivity to dihydropyridines. The cytoplasmic loop between repeats II and III of the  $\alpha_{1S}$  subunit interacts closely with RyR1 and is an important determinant of skeletal type EC coupling [4,5]. A region in the cytoplasmic loop between repeats I and II of the  $\alpha_1$  subunit, referred to as the AID [6], binds tightly with a 30 amino acid region on the  $\beta_1$  subunit, referred to as the BID [7].  $\beta$  subunits are ~ 55 to 65 kDa proteins essential for channel assembly and/or membrane targeting, as well as for modulation of channel kinetics [8]. The  $\alpha_2$ - $\delta$  subunit is a highly glycosylated ~ 175 kDa protein formed by two disulfide-linked peptides encoded by the same gene. Transmembrane topology and functional analyses suggest the  $\alpha_2$ - $\delta$  subunit is composed of a single transmembrane domain and a short cytoplasmic tail of only five residues [9,10]. Given this topology, the  $\alpha_2$ - $\delta$  subunit is most likely to interact with the  $\alpha_1$  and/or the  $\gamma_1$  subunits. The  $\gamma_1$  subunit is a ~ 32 kDa skeletal muscle-specific protein with four presumptive transmembrane domains [11,12,13]. The transmembrane topology of the  $\gamma_1$  subunit and the critical binding domains are unknown at this time.

EC coupling is initiated by voltage-dependent charge movements in the S4 segments of the DHPR  $\alpha_{1S}$  subunit, whose expression is dependent on the presence of the  $\beta_{1a}$  subunit [14]. The C-terminus of the  $\beta_{1a}$  subunit has also been shown to be important in EC coupling, presumably by interaction with RyR1 [15]. The role of the  $\alpha_2$ - $\delta$  subunit on skeletal EC coupling is unknown, but in heterologous expression systems it has been demonstrated to increase the amount of charge movement [16]. The role of the  $\gamma_1$  subunit in  $Ca^{2+}$  channel function is of particular interest given the discovery of a second  $\gamma$  subunit,  $\gamma_2$  or *stargazin*, which is expressed in neurons and is responsible for the *stargazer* mutation in mice [17]. Subsequently, several other  $\gamma$  subunit genes have been identified and shown to be expressed in brain and peripheral tissues [18,19]. In the present study we examined the role of the  $\gamma_1$  subunit in L-type  $Ca^{2+}$  current and EC coupling in skeletal myotubes. Absence of the  $\gamma_1$  subunit slows inactivation and produces a depolarizing shift in the  $Ca^{2+}$  current inactivation vs. voltage curve, in

agreement with results from an independently produced  $\gamma_1$  knockout mouse [20]. However, absence of  $\gamma_1$  does not affect the voltage dependence or the magnitude of charge movements and  $Ca^{2+}$  transients. Overall, the  $\gamma_1$  subunit appears to promote inhibition of the  $Ca^{2+}$  channel function of the skeletal DHPR. While this subunit is clearly non-essential for activation of the L-type  $Ca^{2+}$  channel and for triggering skeletal-type EC coupling,  $\gamma_1$  appears to specifically modulate the  $Ca^{2+}$  channel function of the skeletal DHPR.

## Results and Discussion

### **Inactivation of the DHPR $\gamma_1$ subunit by gene targeting**

Gene targeting was used to replace the entire coding region of the  $\gamma_1$  gene with the *neo* gene, as described in Materials and Methods (Fig. 1). Targeted ES cell clones were injected into C57Bl/6J blastocysts and chimeras obtained. After additional breeding, a line containing the  $\gamma_1$  targeted allele was obtained. Fig. 1A shows Southern blots from DNA of control (+/+),  $\gamma_1$  het (+/-) and  $\gamma_1$  null (-/-) mice, after digestion with *EcoRI* and hybridization to probe 1. The  $\gamma_1$  het and  $\gamma_1$  null mice show the predicted 12.5 kb restriction fragment indicative of the targeted allele (Fig. 1B). Similarly for the Southern blot of DNA digested with *HindIII* and hybridized to probe 2, the  $\gamma_1$  het and  $\gamma_1$  null mice show the predicted 3.5 kb restriction fragment indicative of the targeted allele (Fig. 1C). The  $\gamma_1$  het and  $\gamma_1$  null mice have no visible abnormalities and are fertile. Western blots showing the expression of the DHPR subunits are shown in Fig 1D. The amount of the  $\gamma_1$  subunit present in control,  $\gamma_1$  het and  $\gamma_1$  null samples as a function of total membrane protein was determined in two independent membrane preparations. These data indicate that the amount of  $\gamma_1$  expression in membranes from  $\gamma_1$  null muscle was not detectable above background (no primary antibody) as expected from the fact that the entire gene was deleted. In membranes isolated from the  $\gamma_1$  het mice, the level of expression of the  $\gamma_1$  subunit was 64% of control values for each of the two independent determinations, consistent with what might be expected from the loss of one allele. Whether there is compensation by increased expression of other  $\gamma$  subunits such as the  $\gamma_6$  and  $\gamma_7$  subunits, which were shown recently to be present in skeletal muscle by RT-PCR [19], or alteration of the amount of the other subunits remains to be determined in the future.

### **Increase in $Ca^{2+}$ current density and decrease in inactivation in $\gamma_1$ null and $\gamma_1$ het myotubes**

We examined the impact of the  $\gamma_1$  null mutation on DHPR properties using electrophysiological techniques in primary cultures of skeletal myotubes derived from mouse embryos. Fig. 2A shows whole-cell  $Ca^{2+}$  currents in control,  $\gamma_1$  het and  $\gamma_1$  null myotubes in response to 500-ms depolarizing voltage steps from a holding poten-

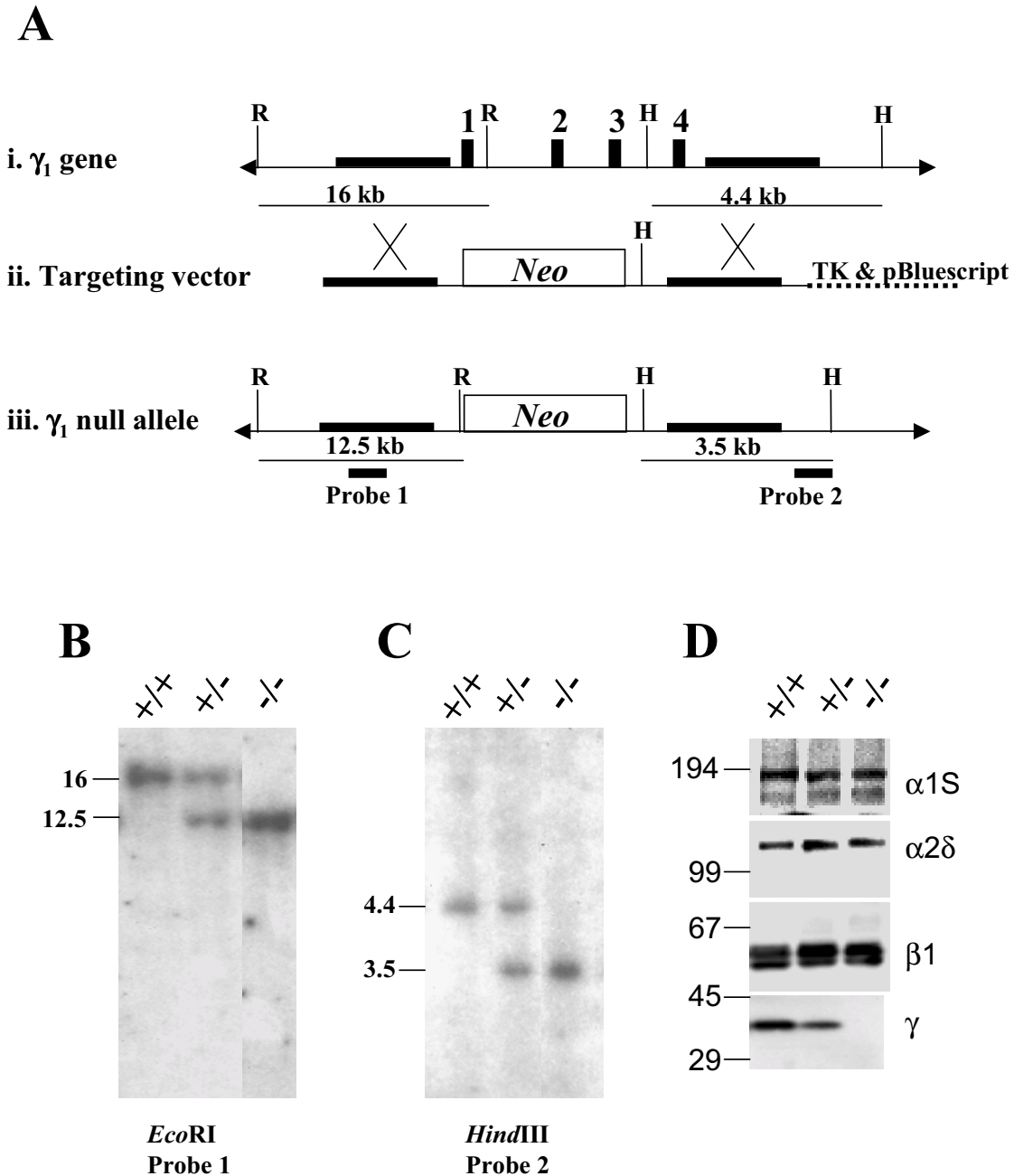


**Figure 1**  
**Inactivation of the  $\gamma_1$  subunit by gene targeting.** A) i. The normal  $\gamma_1$  gene, which contains 4 exons (represented by black boxes). ii. The targeting vector contains a fragment with 4.4 kb of homology to a region 5' of exon 1 and a 2.6 kb fragment with homology to a region 3' of exon 4 (thick horizontal lines). These fragments are separated by the *neo* gene, which is used to select the ES cells in culture. iii. The modified  $\gamma_1$  locus. When recombination occurs in the regions indicated by the X's, all 4 exons of the  $\gamma_1$  gene are replaced by the *neo* cassette. B, C) Southern blots of DNA, either digested with *EcoRI* and hybridized to probe 1 (B), or DNA digested with *HindIII* and hybridized to probe 2 (C), from control (+/+),  $\gamma_1$  het (+/-) and  $\gamma_1$  null (-/-) mice. These data show the predicted size bands for the wild type and targeted alleles. D) Western blots for each of the four skeletal DHP subunits from control (+/+),  $\gamma_1$  het (+/-) and  $\gamma_1$  null (-/-) mice. The  $\gamma_1$  subunit is absent from the  $\gamma_1$  null mice and at approximately half the normal level in the  $\gamma_1$  het mice.

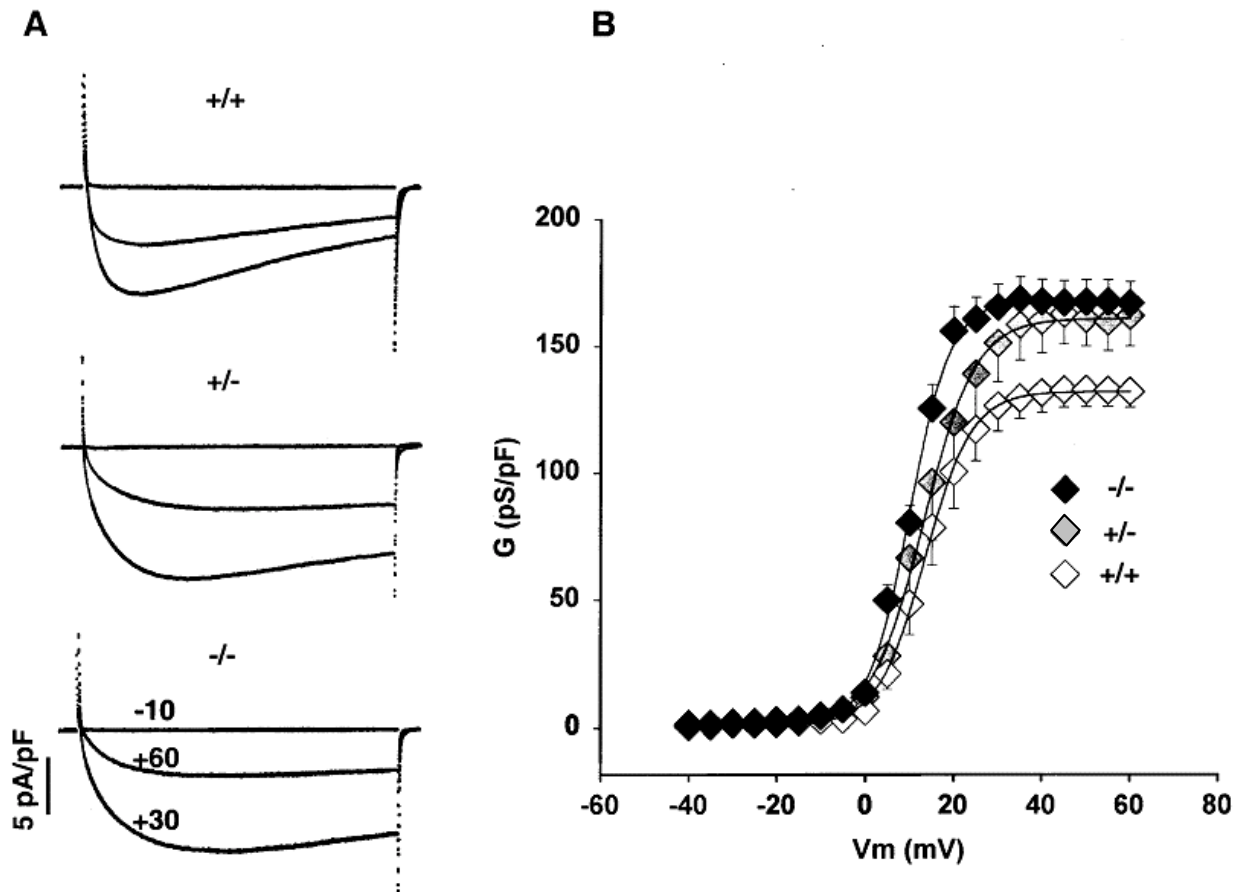


**Figure 2**

**L-type  $\text{Ca}^{2+}$  conductance in  $\gamma_1$  knockout myotubes.** A) Whole-cell L-type  $\text{Ca}^{2+}$  current when control (+/+),  $\gamma_1$  het (+/-), or  $\gamma_1$  null (-/-) myotubes are depolarized to either -10 mV, +30 mV or +60 mV from a holding potential of -40 mV. The pulse duration was 500 ms. The cell capacitance was 262 pF, 221 pF, and 286 pF, for the control,  $\gamma_1$  het and  $\gamma_1$  null cells, respectively. B) Voltage dependence of the  $\text{Ca}^{2+}$  conductance for 8 control, 8  $\gamma_1$  het and 12  $\gamma_1$  null cells. The curves correspond to a Boltzmann fit of the population mean with the following parameters.  $G_{\max} = 132$  pS/pF,  $V_{1/2} = 13.4$  mV and  $k = 5.3$  mV for control cells;  $G_{\max} = 160$  pS/pF,  $V_{1/2} = 13$  mV and  $k = 5.8$  mV for  $\gamma_1$  het cells; and  $G_{\max} = 167$  pS/pF,  $V_{1/2} = 9.9$  mV and  $k = 4.6$  mV for  $\gamma_1$  null cells.

tial of -40 mV. Current traces for only three voltage steps are shown for clarity. All three cell types displayed the slow, high-voltage activated L-type  $\text{Ca}^{2+}$  current typical of skeletal myotubes. When the holding potential was -80 mV, we also observed a T-type  $\text{Ca}^{2+}$  current, which was seen in approximately half of the cells tested (data not shown).  $\text{Ca}^{2+}$  conductance vs. voltage curves were computed in Fig. 2B for the three cell types. The sigmoidal lines correspond to a Boltzmann fit to the population mean while parameters fitted to each cell are shown in Table 1. These data show that the maximum conductance,  $G_{\max}$ , for both the  $\gamma_1$  het and  $\gamma_1$  null cells are significantly larger ( $p < 0.05$ ) than the values for control cells.

However, the half-activation potential ( $V_{1/2}$ ) and the steepness of the curve (factor  $k$ ) were not significantly different (see Table 1). Thus, full or partial elimination of the  $\gamma_1$  subunit produced a significant increase in the  $\text{Ca}^{2+}$  current density without a change in the voltage-dependence of the  $\text{Ca}^{2+}$  conductance.

At intermediate potentials such as +30 mV (Fig. 2A), the  $\text{Ca}^{2+}$  current of  $\gamma_1$  het and  $\gamma_1$  null cells inactivated more slowly than that of control cells. To examine changes in inactivation, we used the paired-pulse protocol shown in Fig. 3A, which measured the  $\text{Ca}^{2+}$  current not inactivated by the pre-pulse. It has been shown that inactivation of

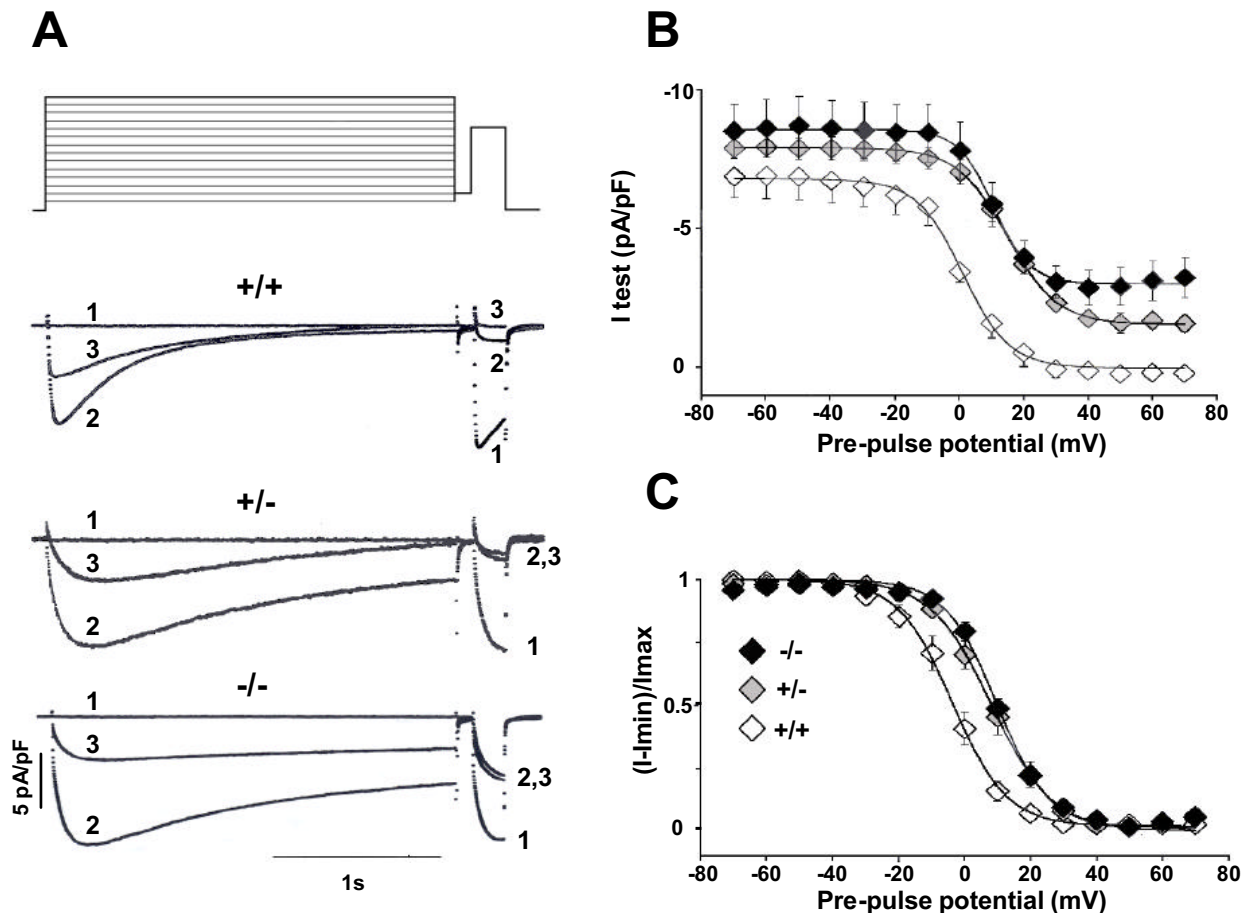


**Figure 3**

**Slow inactivation of the  $\text{Ca}^{2+}$  current in  $\gamma_1$  knockout myotubes.** A) Diagram to scale of the two-pulse protocol used to inactivate the L-type  $\text{Ca}^{2+}$  current at each of 15 potentials and then the test potential (+20 mV) to measure the remaining non-inactivated current.  $\text{Ca}^{2+}$  currents during the pre-pulse and test-pulse phases of the protocol are shown for a pre-pulse depolarization to -70 mV (trace 1), +30 mV (trace 2) and +60 mV (trace 3) in a control, a  $\gamma_1$  het, and a  $\gamma_1$  null myotube. The cell capacitance was 317 pF for the control, 175 pF for the  $\gamma_1$  het and 348 pF for the  $\gamma_1$  null cell. B) The maximum  $\text{Ca}^{2+}$  current during the test pulse is plotted as a function of the pre-pulse potential for 6 control, 8  $\gamma_1$  het and 8  $\gamma_1$  null cells. C) The non-inactivating component was subtracted and the curves were normalized to show the voltage-dependence of the inactivating component.  $I$  is the maximum test current,  $I_{\text{min}}$  is the test current at +50 mV and  $I_{\text{max}}$  is the test current at -70 mV. The curves correspond to a Boltzmann fit of the population mean with the following parameters.  $[(I - I_{\text{min}}) / I_{\text{max}}]_{\text{max}} = 1$ ,  $V_{1/2} = -3.8$  mV and  $k = 8.4$  mV for control cells.  $[(I - I_{\text{min}}) / I_{\text{max}}]_{\text{max}} = 1$ ,  $V_{1/2} = +15.6$  mV and  $k = 8.1$  mV for  $\gamma_1$  het cells.  $[(I - I_{\text{min}}) / I_{\text{max}}]_{\text{max}} = 1$ ,  $V_{1/2} = +9.7$  mV and  $k = 7.9$  mV for  $\gamma_1$  null cells.

skeletal L-type  $\text{Ca}^{2+}$  channels approaches steady-state extremely slowly, on the time scale of tens of seconds [21]. However, for comparative purposes and to be consistent with previous measurements in  $\text{Ca}^{2+}$  channels lacking  $\gamma_1$  [20,22], we chose a much shorter protocol. Cells were held at -80 mV, then stepped to a series of depolarizing (pre-pulse) voltages for 2.5 s to promote inactivation, then stepped to -50 mV for 100 ms to close

non-inactivated channels. The non-inactivated  $\text{Ca}^{2+}$  current was measured during a 200-ms test pulse to +20 mV. In control cells, there was almost complete inactivation of the  $\text{Ca}^{2+}$  current when the pre-pulse potential was in the positive range. This can be seen by comparing the amplitude of the  $\text{Ca}^{2+}$  current during the test pulse in traces 1, 2, and 3, corresponding to pre-pulse potentials to -70 mV, +30 mV, and +60 mV, respectively. In con-

**Table 1: Boltzmann parameters of Ca<sup>2+</sup> conductance, charge movements and Ca<sup>2+</sup> transients of control,  $\gamma_1$  het and  $\gamma_1$  null myotubes.**

CELL TYPE	G-V			Q-V		
	G <sub>max</sub> (pS/pF)	V <sub>1/2</sub> (mV)	k (mV)	Q <sub>max</sub> (fC/pF)	V <sub>1/2</sub> (mV)	k (mV)
<b>Control, +/+</b> (n)	131 ± 6.2 (8)	14.7 ± 2.1	4.2 ± 0.4	5.3 ± 0.4 (8)	11.4 ± 2.5	15.4 ± 1.1
$\gamma_1$ <b>het, +/-</b> (n)	161 ± 11.5 <sup>a</sup> (8)	14.3 ± 2.8	5 ± 0.8	5.3 ± 0.3 (4)	14.4 ± 0.6	14.7 ± 2.0
$\gamma_1$ <b>null, -/-</b> (n)	170 ± 9.6 <sup>b</sup> (12)	10.9 ± 0.9	4.5 ± 0.4	5.3 ± 0.9 (8)	17.8 ± 1.9	15.8 ± 2.2

	$\Delta F/Fo-V$			Inactivation	
	$\Delta F/Fo_{(max)}$	V <sub>1/2</sub> (mV)	k (mV)	V <sub>1/2</sub> (mV)	k (mV)
<b>Control, +/+</b> (n)	3.9 ± 0.3 (6)	4.6 ± 1.2	10.2 ± 1.3	-4.6 ± 3.6 (6)	7.3 ± 0.2
$\gamma_1$ <b>het, +/-</b> (n)	3.3 ± 0.5 (4)	8.2 ± 3.0	10.1 ± 2.0	8.1 ± 2.3 <sup>c</sup> (8)	8.0 ± 0.6
$\gamma_1$ <b>null, -/-</b> (n)	3.7 ± 0.4 (6)	7.3 ± 1.6	9.0 ± 1.1	8.9 ± 0.8 <sup>d</sup> (8)	8.1 ± 0.8

Entries (mean ± SEM) correspond to Boltzmann parameters fitted to each cell (number of cells n, in parenthesis). The only statistically significant differences ( $p < 0.05$ ) were for either  $\gamma_1$  het or  $\gamma_1$  null cells compared to control cells as indicated. The t-test p values were 0.004, 0.009, 0.011, 0.009 for a-d, respectively.

trast,  $\gamma_1$  het and  $\gamma_1$  null cells showed less inactivation during the pre-pulse, and thus a significantly larger Ca<sup>2+</sup> current during the test pulse. Furthermore, pre-pulse potentials larger than +30 mV did not promote additional inactivation, which can be seen by comparing traces 2 and 3 in the  $\gamma_1$  het and  $\gamma_1$  null cells. Fig. 3B shows the maximum Ca<sup>2+</sup> current during the test pulse plotted as a function of the pre-pulse potential. In control cells, inactivation was complete when the pre-pulse potential was above +30 mV (-6.9 ± 0.8 pA/pF at -70 mV vs. -0.2 ± 0.2 pA/pF at +70 mV, n = 6 cells). In  $\gamma_1$  null cells, inactivation reached a plateau when the pre-pulse potential was more positive than +20 mV (-8.5 ± 0.9 pA/pF at -70 mV vs. -3.2 ± 0.7 pA/pF at +70 mV, n = 8 cells). Incomplete inactivation was also seen in  $\gamma_1$  het cells, although this was less pronounced than in  $\gamma_1$  null cells. Since the pre-pulse was not sufficiently long for inactivation to reach steady-state, we are not certain whether the observed incomplete inactivation reflects a component of the  $\gamma_1$  null Ca<sup>2+</sup> current that inactivates extremely slowly or a "truly" non-inactivating component. To compare the voltage-dependence of the inactivation produced by the 2.5-

second pre-pulse, the Ca<sup>2+</sup> current during the test pulse was normalized and fit to the Boltzmann equation (Fig. 3C). The curves for  $\gamma_1$  het and  $\gamma_1$  null cells showed a significant ( $p < 0.05$ ) shift to more positive potentials compared to control cells. The same conclusion was reached by comparing the Boltzmann parameters of individual cells in Table 1. Since control cells had a more negative half inactivation potential, the higher Ca<sup>2+</sup> conductance of  $\gamma_1$  het and  $\gamma_1$  null cells reported in Fig. 2 could be explained by a larger steady-state inactivation of the control Ca<sup>2+</sup> current at the -40 mV holding potential. To determine if this was the case, we measured the Ca<sup>2+</sup> conductance during the pre-pulse for the same cells analyzed in Fig 3B,C. The pre-pulse was delivered from a holding potential of -80 mV, and therefore the pre-pulse current should be less contaminated by steady-state inactivation. G<sub>max</sub> at the peak of the Ca<sup>2+</sup> current during the pre-pulse was 146 ± 12 pS/pF for controls, 172 ± 18 pS/pF  $\gamma_1$  het and 186 ± 13 pS/pF for  $\gamma_1$  null cells with t-test statistical significance for controls vs.  $\gamma_1$  null cells of  $p = 0.034$  and for controls vs.  $\gamma_1$  het cells of  $p = 0.064$ . Thus the higher Ca<sup>2+</sup> conductance of  $\gamma_1$  het and  $\gamma_1$  null

cells persisted at the more negative holding potential. These  $\text{Ca}^{2+}$  conductances were approximately 10% higher than those at the -40 mV holding potential reported in Table 1. The additional current could have been contributed by T-type  $\text{Ca}^{2+}$  channels (not shown), which are available at the -80 mV holding potential but are inactivated at the more positive holding potential. Also, since the T-type  $\text{Ca}^{2+}$  current density was highly variable (see above), this could explain the higher p values compared to those reported in Table 1. In summary, decreasing the amount of the  $\gamma_1$  subunit protein or eliminating it completely resulted in myotubes with a higher  $\text{Ca}^{2+}$  current density, a similar voltage-dependence of activation, and a reduced rate of inactivation. These results, with the exception of the change in  $\text{Ca}^{2+}$  current density, are in remarkable agreement with those obtained when L-type  $\text{Ca}^{2+}$  channel subunits are coexpressed without the  $\gamma_1$  subunit in heterologous cells (see below). They also are similar to results obtained elsewhere in  $\gamma_1$  null myotubes using a 5-second pre-pulse [20]. Furthermore, the incomplete inactivation of the  $\gamma_1$  null  $\text{Ca}^{2+}$  current resembles that observed in ts A201 cells expressing DHPRs specifically lacking  $\gamma_1$  and using a 3-second inactivation protocol [22].

The effect of the  $\gamma_1$  subunit on  $\text{Ca}^{2+}$  current kinetics has been somewhat confusing until now, because it has not been possible to examine its role using homologous subunits and a homologous expression system. In amphibian oocytes,  $\gamma_1$  was assayed in a complex with  $\alpha_{1C}$ ,  $\beta_{1a}$  and  $\alpha_2\text{-}\delta$  [23,24]. These investigators found  $\gamma_1$  produced a slight decrease in  $\text{Ca}^{2+}$  current density, no change in activation kinetics and a positive shift in the peak  $\text{Ca}^{2+}$  current vs. voltage curve. In HEK293 cells using the same subunit composition, the  $\gamma_1$  subunit did not alter the kinetics or density of  $\text{Ca}^{2+}$  currents [25]. However, in both oocytes and HEK293 cells, the  $\gamma_1$  subunit increased the rate of  $\text{Ca}^{2+}$  channel inactivation and produced a large hyperpolarizing shift in steady-state inactivation [23,25,26]. The results obtained here in skeletal muscle demonstrate that absence of the  $\gamma_1$  subunit increases  $\text{Ca}^{2+}$  current density, decreases the inactivation rate, and shifts the voltage-dependence of inactivation in the depolarizing direction. Freise et al. [20] showed that the increase in  $\text{Ca}^{2+}$  current was not a result of changes in single channel conductance and suggested the effects were due to changes in channel open probability. However, this remains to be tested directly. Expression of the  $\gamma_2$  subunit in BHK cells expressing  $\alpha_{1A}$ ,  $\alpha_2\text{-}\delta$  and  $\beta_{1a}$  also shifts the voltage-dependence of inactivation  $\sim 7$  mV in the hyperpolarizing direction [17]. In summary, the two  $\gamma$  subunits that have been characterized to date, namely  $\gamma_1$  in the homologous skeletal myotube system described here and  $\gamma_2$  described above in heterologous BHK cells [17], appear to be inhibitory. In each case, the presence

of  $\gamma$  results in fewer  $\text{Ca}^{2+}$  channels available for activation.

#### **Absence of changes in the EC coupling voltage sensor of $\gamma_1$ null myotubes**

The impact of the  $\gamma_1$  null mutation on myotube EC coupling was inferred from intramembrane charge movements, the bulk of which have been shown to originate from the DHPR voltage sensor [27,28]. Additionally, we measured  $\text{Ca}^{2+}$  transients evoked by voltage (i.e., by the movement of the voltage sensor) and compared these two sets of data. To measure DHPR charge movements and to separate these charge movements from those produced by other voltage-gated channels, a) ionic currents were blocked; b) the linear component of the cell capacity was subtracted using a P/4 procedure and by analog compensation; and c) we used a pulse protocol that eliminated the immobilization-sensitive charge movements from voltage-gated  $\text{Na}^+$  channels and presumably also from T-type  $\text{Ca}^{2+}$  channels. Previous studies in dysgenic ( $\alpha_{1S}$  null) myotubes transfected with  $\alpha_{1S}$  showed that the pulse protocol and the internal and external solutions used here (see Materials and Methods) detected charge movements of a magnitude 5 to 8 fold larger than those present in non-transfected dysgenic myotubes [28]. Thus we are confident that the technique adequately measures intramembrane charge movements in DHPR voltage sensors present in the plasma membrane. Fig. 4A shows "gating-type" currents produced by charge movements in response to 3 of 14 step voltages delivered to each cell (-40, +10, and +70 mV). Charge movements did not occur at -40 mV in any of the cell types. Traces at +10 mV and +70 mV show a transient current at the onset of the voltage step, the ON charge, and an equal inverted current at the end of the voltage step, the OFF charge. The voltage-dependence of the OFF charge estimated by integration is shown in Fig. 4B. The OFF transient was usually less contaminated by ionic current than the ON transient, and for that reason it provides a better estimate of the total DHPR charge. The main contaminant of the ON transient was a non-linear outward current, presumably a  $\text{K}^+$  channel that was not always completely blocked by the pipette solution. The OFF charge increased in a sigmoidal fashion and saturated at potentials more positive than +60 mV in all cases. These data were adequately fit by a Boltzmann equation shown by the lines. We found that the fitted maximum charge ( $Q_{\text{max}}$ ) expressed by the 3 cell types was  $\sim 5$  fC/pF, in agreement with previous determinations in normal myotubes [29]. Furthermore, Boltzmann parameters determined for each cell and then averaged were not significantly different in any of two-by-two comparisons between control,  $\gamma_1$  het or  $\gamma_1$  null cells (Table 1). In summary, the magnitude of intramembrane charge movements and its voltage dependence were unaltered by

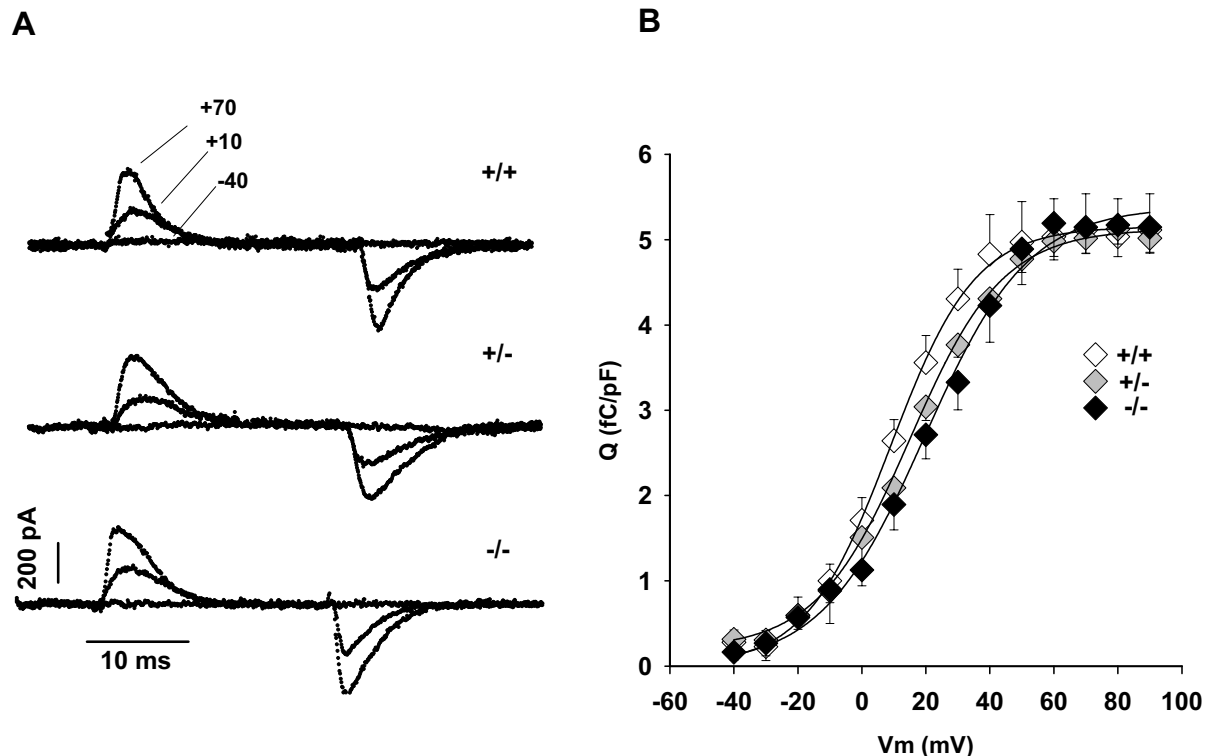


**Figure 4**

**Voltage dependence of intramembrane charge movements in  $\gamma_1$  knockout myotubes.** A) Whole-cell current produced by charge movements in response to 3 of 14 25-ms voltage steps delivered to the same cell. The voltage steps shown are to -40 mV, +10 mV, and +70 mV. The cell capacitance was 241 pF for the control, 292 pF for the  $\gamma_1$  het and 253 pF for the  $\gamma_1$  null cell. B) Voltage dependence of charge movement obtained by integration of the OFF transient current for 8 control, 4  $\gamma_1$  het, and 8  $\gamma_1$  null cells. The curves correspond to a Boltzmann fit of the population mean with the following parameters.  $Q_{\max} = 5.2$  fC/pF,  $V_{1/2} = 13.2$  mV and  $k = 9$  mV for control cells.  $Q_{\max} = 4.9$  fC/pF;  $V_{1/2} = 15$  mV and  $k = 14.5$  mV for  $\gamma_1$  het cells.  $Q_{\max} = 5.4$  fC/pF,  $V_{1/2} = 19.6$  mV and  $k = 16$  mV for  $\gamma_1$  null cells.

partial or complete removal of the  $\gamma_1$  subunit. Furthermore, in agreement with previous data [29], no additional charges moved when pulses were delivered from a holding potential of -120 mV (data not shown). Thus, failure to detect changes in the charge vs. voltage characteristics of  $\gamma_1$  null myotubes compared to controls cannot be explained by charge movements in the  $\gamma_1$  null myotubes occurring at potentials more negative than the chosen -80 mV holding potential.

Absence of alterations in the voltage dependence of charge movement in the  $\gamma_1$  null cells should also be reflected in the voltage-dependence of  $\text{Ca}^{2+}$  transients. Changes in intracellular  $\text{Ca}^{2+}$  were measured using confocal line-scan imaging of fluo-4 fluorescence. Fig. 5A shows a line-scan image of a  $\text{Ca}^{2+}$  transient stimulated by a 50 ms depolarization to +90 mV from a holding po-

tential of -40 mV in each cell type. The scan direction was perpendicular to the long axis of the myotube in a region selected on the basis of a low resting fluorescence and a high stimulated fluorescence (red/yellow color). The two traces on top of each image correspond to the time course of the fluo-4 fluorescence averaged across the entire line-scan at -10 mV, which is close to the threshold, and at +90 mV, which produced the maximum  $\text{Ca}^{2+}$  transient. Increase in cytosolic  $\text{Ca}^{2+}$  started at the onset of the depolarization and peaked ~ 100 ms later in the three cell types. For all cells, the peak fluorescence change for the depolarization to +90 mV was  $>3 \Delta F/\text{Fo}$  units, which is equivalent to  $>4$  times the resting fluorescence. The relatively long recovery time following the depolarization is due to the low  $\text{Ca}^{2+}$  buffering power of the internal recording solution and is in agreement with previous studies [27,30]. The voltage dependence of  $\Delta F/\text{Fo}$



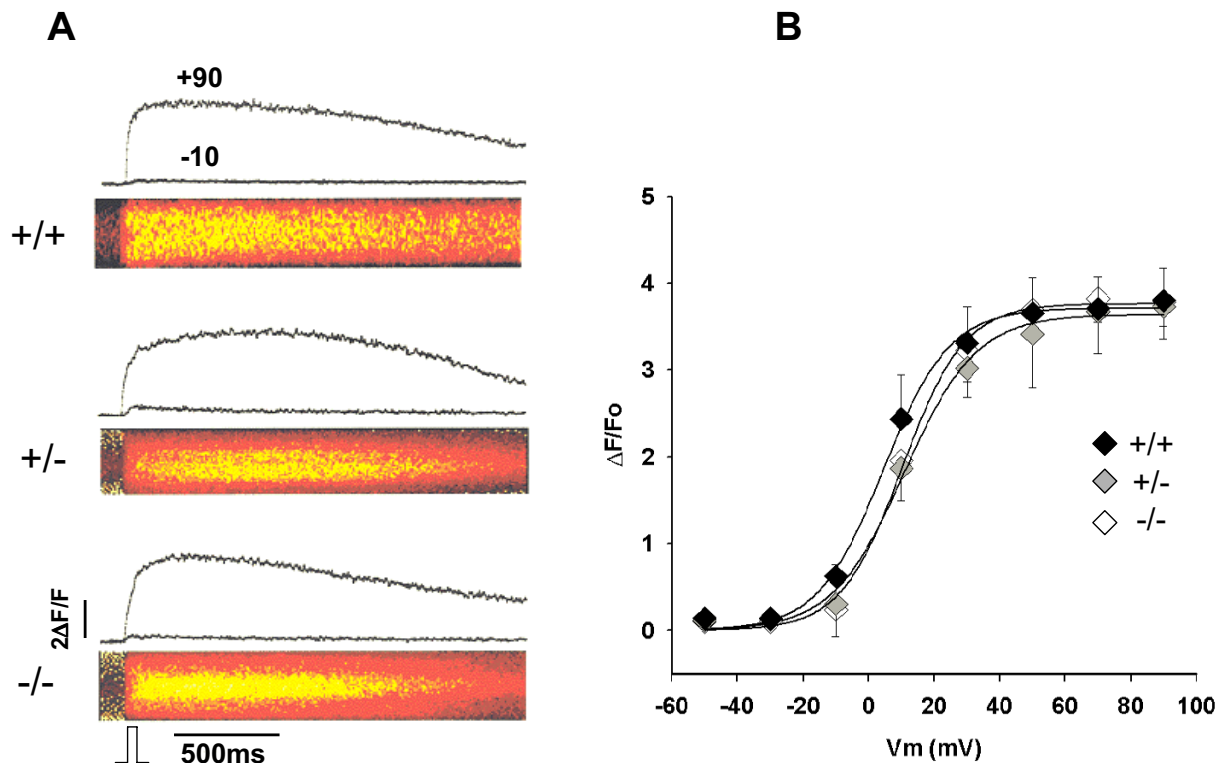


**Figure 5**

**Voltage-dependence of  $\text{Ca}^{2+}$  transients in  $\gamma_1$  knockout and normal myotubes.** A) Confocal line-scan images of fluo-4 fluorescence in response to a 50 ms step to +90 mV from a holding potential of -40 mV. Hot colors represent high fluorescence (yellow>red). The pulse was delivered 100 ms after the start of the line-scan as indicated at the bottom of the figure. Images have a horizontal dimension of 2.05 seconds in all cases. The vertical dimension was 15, 28, and 24 microns for the control,  $\gamma_1$  het, and  $\gamma_1$  null cells, respectively. The two curves on top of the image show the time course of the fluorescence intensity at -10 mV and +90 mV. 1  $\Delta\text{F}/\text{F}_0$  unit corresponds to a doubling of the cell resting fluorescence. B) Voltage-dependence of the peak  $\Delta\text{F}/\text{F}_0$  for 6 control, 4  $\gamma_1$  het, and 6  $\gamma_1$  null cells. The curves correspond to a Boltzmann fit of the population mean with the following parameters.  $\Delta\text{F}/\text{F}_{0\text{max}} = 3.8$ ,  $V_{1/2} = 10$  mV,  $k = 9.4$  mV for control cells.  $\Delta\text{F}/\text{F}_{0\text{max}} = 3.6$ ,  $V_{1/2} = 10.8$  mV;  $k = 10.9$  mV for  $\gamma_1$  het cells.  $\Delta\text{F}/\text{F}_{0\text{max}} = 3.7$ ,  $V_{1/2} = 4.5$  mV;  $k = 10$  mV for  $\gamma_1$  null cells.

measured at the peak of the transient is shown in Fig. 5B. All curves had the same profile which consisted of a threshold for peak  $\text{Ca}^{2+}$  release at -10 mV, an increase in peak  $\text{Ca}^{2+}$  with pulse potential from -10 mV to +30 mV and a plateau at more positive potentials. Furthermore, two-by-two comparisons of Boltzmann parameters fitted to each cell did not reveal statistically significant differences (see Table 1). In summary, the voltage-dependence of  $\text{Ca}^{2+}$  transients and the maximum cytosolic  $\text{Ca}^{2+}$  concentration during the transient were not significantly affected by partial or total absence of the  $\gamma_1$  subunit. However, we cannot rule out changes in the rate of SR  $\text{Ca}^{2+}$  release since this measurement requires an entirely different internal solution [31]. A recent report indicates

that the SR  $\text{Ca}^{2+}$  release rate is slightly higher in  $\gamma_1$  null myotubes [32].

#### **Involvement of DHPR subunits in voltage sensing and EC coupling**

The  $\alpha_{1S}$  pore subunit of the skeletal DHPR is the main determinant of charge movements and EC coupling [4,27,28]. However, other subunits of the DHPR are critical modulators of both functions. In heterologous expression systems, the  $\alpha_2$ - $\delta$  subunit was shown to affect the rate of  $\text{Ca}^{2+}$  current inactivation and charge movement immobilization [33]. Studies investigating the role of the  $\beta$  subunit on charge movement vary with the expression system used. In amphibian oocytes,  $\beta$  subunits increase the coupling between charge movements and

channel opening [34,35]. We have shown in skeletal muscle cells lacking the  $\beta_1$  subunit that reintroduction of variants of  $\beta_1$  has little effect on either charge movement or the kinetics of activation of the expressed  $\text{Ca}^{2+}$  current [15]. However, the carboxyl terminus of  $\beta_1$  is an important determinant of the efficiency of the coupling between charge movement and  $\text{Ca}^{2+}$  release [15]. In contrast to these results, earlier studies in which similar  $\beta$  subunits were co-expressed with  $\alpha_1$  subunits in oocytes indicated  $\beta$  subunits had major effects on  $\text{Ca}^{2+}$  current density and gating kinetics [36,37]. While the reason for these discrepancies is unknown, they highlight the fact that in skeletal muscle, the gating characteristics of the L-type  $\text{Ca}^{2+}$  channel might be controlled by interactions beyond those taking place among subunits of the DHPR. For example, a region of RyR1 has been shown to be essential for L-type  $\text{Ca}^{2+}$  current expression [38]. Such interaction is critical for skeletal DHPR function and is unlikely to occur in heterologous expression systems.

## Conclusions

The ability of the  $\gamma_1$  subunit to selectively modulate the pore function of the DHPR without modulation of charge movements or the voltage dependence of  $\text{Ca}^{2+}$  transients is unique, especially since other DHPR subunits participate in both functions. In all likelihood, the charge movement protocol failed to detect gating currents responsible for opening the  $\text{Ca}^{2+}$  channel, which are quite small and are only resolved for depolarizations >200 ms [39] compared to the 25 ms used here (Fig. 4). A possible shift in the voltage-dependence of these charges recruited by long depolarizations would be consistent with the shift in  $\text{Ca}^{2+}$  current inactivation and remains to be resolved in  $\gamma_1$  null myotubes. However, the protocol accurately measures the immobilization-resistant charge movements that are known to be required for skeletal-type EC coupling [31,40]. Therefore, the  $\gamma_1$  subunit is unlikely to play a critical role in the activation of SR  $\text{Ca}^{2+}$  release, in agreement with a recent report [32]. However, shifts in voltage dependence below the limit of resolution (see Materials and Methods) and effects on charge movement and  $\text{Ca}^{2+}$  release inactivation cannot be completely ruled out. The  $\gamma_1$  knockout mice provide a unique resource to understand the function of this protein in myotubes in molecular detail.

## Materials and Methods

### Gene targeting

Bacteriophage clones containing portions of the  $\gamma_1$  gene were isolated from a mouse 129Sv genomic library (Stratagene, La Jolla, CA #946305). To inactivate the  $\gamma_1$  gene, a 4.4 kb *Bam*HI/*Xho*I fragment upstream of exon 1 was subcloned into a multiple cloning site 5' of the *neo* and Herpes virus TK gene that was in pBluescript (Stratagene). A second 2.6 kb *Eco*RI/*Bam*HI fragment 3' of

exon 4 of the  $\gamma_1$  gene was cloned into a site between the *neo* and TK genes (Fig. 1Aii). Thus, the targeting vector contains 4.4 kb of identity with the native  $\gamma_1$  gene 5', and 2.6 kb of identity 3' of the *neo* cassette, respectively. The targeting vector also contains the HSV TK gene to allow for negative selection of non-recombinants. A unique *Bam*HI restriction site was used to linearize the plasmid prior to its introduction into mouse ES cells by electroporation. The  $\gamma_1$  gene contains 4 exons, and correct targeting results in the deletion of all 4 exons, which will inactivate the gene (Fig. 1Aiii). Probe 2 was used for identification of targeted clones [41]. 5  $\mu\text{g}$  of the targeting vector was electroporated into  $5 \times 10^6$  AB1 ES cells. G418 and FIAU (1-(2'-deoxy-2'-fluoro- $\gamma$ -D-arabinofuranosyl)-5-iodouracil) resistant clones were analyzed by Southern blotting after digestion with either *Eco*RI and hybridization to probe 1 or digestion with *Hind*III and hybridization to probe 2 (Fig. 1). Of three clones targeted on the 5' end, two also were targeted on the 3' end. These were expanded and used to produce germline chimeras. Mice homozygous for the targeted allele were viable, with no apparent abnormalities. Mice heterozygous and homozygous for the targeted mutation are referred to as  $\gamma_1$  het and  $\gamma_1$  null, respectively.

### Western blots

Total microsomes were prepared from the forelimb and hind limb muscles of control,  $\gamma_1$  het, and  $\gamma_1$  null adult mice as previously described [42]. Total microsomes were washed twice with 0.6 M KCl buffer and 100  $\mu\text{g}$  of total membrane protein was applied to a 5-15% SDS polyacrylamide gel. Proteins were transferred to PVDF membranes and analyzed with either anti- $\alpha_{1S}$  mAb IIC12 antibody [43], or anti- $\alpha_2$ - $\delta$  protein G-purified guinea pig antibody #1 [13], or anti- $\beta_{1a}$  affinity-purified sheep #6 antibody [44], or with anti- $\gamma_1$  affinity-purified guinea pig #16 antibody and the appropriate secondary antibodies [11]. The subunits were visualized using SuperSignal ECL reagent (Pierce, Rockford, IL). The images were captured on a Chemi-Imager (Alpha Innotech, San Leandro, CA) set to a level just below saturation.

### Primary cultures of mouse myotubes

Primary cultures were prepared from hind limbs of day 18 embryos (E18) as described previously [45]. Dissected muscles were incubated for 9 min at 37°C in  $\text{Ca}^{2+}$ / $\text{Mg}^{2+}$ -free Hanks balanced salt solution (in mM: 136.9 NaCl, 3 KCl, 0.44  $\text{KH}_2\text{PO}_4$ , 0.34  $\text{NaH}_2\text{PO}_4$ , 4.2  $\text{NaHCO}_3$ , 5.5 glucose, pH 7.2) containing 0.25% (w/v) trypsin and 0.05 % (w/v) pancreatin (Sigma, St. Louis, MO). Mononucleated cells were resuspended in plating medium containing 78% Dulbecco's modified Eagle's medium (DMEM) with low glucose (Life Technologies, Rockville, MD), 10 % horse serum (HS, Sigma, St. Louis, MO), 10 % fetal bovine serum (FBS, Sigma, St. Louis, MO), 2% chicken em-

bryo extract (CEE, Life Technologies, Rockville, MD) and plated on plastic culture dishes coated with gelatin at a density of  $\sim 1 \times 10^4$  cells per dish. Cultures were grown at 37°C in 8 % CO<sub>2</sub>. After the fusion of myoblasts ( $\sim 7$  days), the medium was replaced with a FBS-free medium (88.75 % DMEM, 10 % HS, 1.25% CEE) and cells were incubated in 5% CO<sub>2</sub>. All media contained 0.1 % v/v penicillin and streptomycin (Sigma, St. Louis, MO). All measurements were made when the cells had been in culture for 7-10 days. During this time the maximal current density did not change [45].

### Electrophysiological measurements

Whole-cell recordings were performed as described previously [29] using an Axopatch 200B amplifier (Axon Instruments, Foster City, CA). Linear capacity and leak currents were compensated with the circuit provided by the manufacturer. Series resistance,  $R_s$ , was compensated up to the point of amplifier oscillation with the Axopatch circuit. Considering all cells in the present study, the linear capacitance (mean  $\pm$  SE) of control,  $\gamma_1$  null, and  $\gamma_1$  het myotubes was  $256 \pm 25$  pF (38 cells),  $246 \pm 16$  pF (34 cells) and  $223 \pm 24$  (23 cells), respectively.  $R_s$  of the same cells before analog compensation was  $7 \pm 0.5$  M $\Omega$ ,  $7.2 \pm 0.4$  M $\Omega$ , and  $6.3 \pm 0.5$  M $\Omega$ , respectively. Following compensation, the effective  $R_s$  was  $<2$  M $\Omega$  in all cases measured, although this was not measured systematically. Considering a mean cell capacitance of 240 pF, a typical maximum current density of 5 to 10 pA/pF (see Fig. 3B), and  $R_s$  (effective)  $<2$  M $\Omega$ , the voltage error was  $<2.4$  to  $<4.8$  mV. All experiments were performed at room temperature. Patch pipettes had an open tip resistance of 1-2 M $\Omega$  when filled with the pipette solution. Ca<sup>2+</sup> currents were measured from a holding potential of -40 mV. Test pulses of 500 ms in 5 mV increments ranged from -40 mV to +60 mV. Ca<sup>2+</sup> conductance vs. voltage curves were obtained by extrapolation of the Ca<sup>2+</sup> current to the reversal potential of the cell. To measure inactivation, cells were held at -80 mV, then stepped to a series of depolarizing (pre-pulse) voltages, from -70 mV to +70 mV in 10 mV increments, for 2.5 seconds to promote inactivation, then stepped to -50 mV for 100 ms to close non-inactivated channels, then stepped for 200 ms to the test potential of +20 mV to measure Ca<sup>2+</sup> currents, then stepped to the -80 mV holding potential for 5 seconds to permit recovery from inactivation. Charge movement was measured using a protocol that eliminated immobilization-sensitive components [15,28,29]. Voltage was stepped from a holding potential of -80 mV to -35 mV for 750 ms, then to -50 mV for 5 ms, then to test potential for 25 ms, then to -50 mV for 30 ms and finally to the -80 mV holding potential. Subtraction of the linear component was assisted by a P/4 procedure following the pulse paradigm listed above. P/4 pulses were separated by 500 ms and had a duration of 25 ms. Previous studies showed

this choice of pulse protocol and internal and external solutions resulted in nifedipine-sensitive charge movements of a magnitude  $\sim 5$  fold larger than those detected in dysgenic myotubes lacking  $\alpha_{1S}$  [29].

### Solutions

The external solution in all cases was (in mM) 130 TEA methanesulfonate, 10 CaCl<sub>2</sub>, 1 MgCl<sub>2</sub>, 10 HEPES titrated with TEA(OH) to pH 7.4. For Ca<sup>2+</sup> transients and Ca<sup>2+</sup> currents, the pipette solution was (in mM) 140 Ca<sup>2+</sup>-Aspartate, 5 MgCl<sub>2</sub>, 0.1 EGTA (Ca<sup>2+</sup> transients) or 5 mM EGTA (Ca<sup>2+</sup> currents), and 10 MOPS-CsOH pH 7.2. For charge movements, the pipette solution was (in mM) 120 NMG (N-methyl glucamine)-Glutamate, 10 HEPES-NMG, 10 EGTA-NMG pH 7.3. For charge movements, the external solution was supplemented with 0.5 mM CdCl<sub>2</sub> and 0.5 mM LaCl<sub>3</sub> to block the Ca<sup>2+</sup> current and 0.05 mM TTX to block residual Na<sup>+</sup> current.

### Ca<sup>2+</sup> transient measurements

Ca<sup>2+</sup> transients were measured using a confocal microscope in line-scan mode as described previously [46,47,48]. Cells were loaded with 4 mM fluo-4 (fluo-4 acetoxymethyl (AM) ester, Molecular Probes, Eugene, OR) for 20 to 40 min at room temperature. Stocks of fluo-4 (1 mg/ml) were made in DMSO and stored frozen. All experiments were performed at room temperature. Cells were viewed with an inverted Olympus microscope with a 20X objective (N.A. = 0.4) and a Fluoview confocal attachment (Olympus, Melville, NY). The 488 nm spectrum line necessary for fluo-4 excitation was provided by a 5 mW argon laser attenuated to 20% with neutral density filters. The fluorescence intensity,  $F$ , was calculated by densitometric scanning of line-scan images and was averaged over the entire width of the cell. The background fluorescence intensity ( $F_0$ ) was averaged in the same manner from areas of the same image prior to the voltage pulse. The fluorescence unit  $\Delta F/F_0$  corresponds to  $(F-F_0)/F_0$ . The limit of fluorescence detection, based on microscope settings and the average resting fluo-4 fluorescence, was  $\sim 0.1 \Delta F/F_0$  units. That is, we could detect a  $\sim 10\%$  change above the cell resting fluorescence. Using a pseudo-ratiometric equation for estimating the cytosolic free Ca<sup>2+</sup> [48] and assuming a resting free Ca<sup>2+</sup> of 100 nM [48], the nominal limit of resolution of free Ca<sup>2+</sup> change was  $\sim 200$  nM.

### Data and error analysis

For each cell, or for the population average, the voltage dependence of charge movements ( $Q$ ), Ca<sup>2+</sup> conductance ( $G$ ), and peak intracellular Ca<sup>2+</sup> ( $\Delta F/F_0$ ) were fitted according to a Boltzmann equation  $A = A_{\max}/(1+\exp(-(V-V_{1/2})/k))$  where  $A_{\max}$  was either  $Q_{\max}$ ,  $G_{\max}$  or  $\Delta F/F_0$ ;  $V_{1/2}$  is the potential at which  $A = A_{\max}/2$ ; and  $k$  is the slope factor. For a fit of steady-state inactivation, the

term ( $V - V_{1/2}$ ) in the equation above was replaced by ( $V_{1/2} - V$ ).  $Ca^{2+}$  conductance for each cell was computed from the extrapolated reversal potential and the maximal  $Ca^{2+}$  current at each voltage. In all figures, the symbols and error bars correspond to the population mean  $\pm 1$  SEM. The curves correspond to a Boltzmann fit of the mean. In addition to Student t-tests reported in Table 1, one-way ANOVA tests were conducted among the 11 sets of Boltzmann parameters of control,  $\gamma_1$  het and  $\gamma_1$  null cells of Table 1. The null hypothesis (equality of means) was not rejected at a level of significance  $p < 0.05$  except in the two cases also identified by t-tests, namely  $G_{max}$  and  $V_{1/2}$  inactivation. An F-test, which formally tests for the difference between the variances of independent populations, was used to determine which of the fitted Boltzmann parameters ( $A_{max}$ ,  $V_{1/2}$ ,  $k$ ) had the largest variance, and thus the largest experimental error. The ranking order in variance error was  $V_{1/2} > A_{max} > k$ . Furthermore, the error in  $V_{1/2}$  was the largest for the fluorescence measurement and the smallest for the conductance measurement. This result was expected since the size of the voltage step used in the  $V_{1/2}$  determination was 5 mV for conductance, 10 mV for charge movements, and 20 mV for fluorescence. The number of voltage steps in fluorescence measurements was kept to a minimum to avoid rundown of the  $Ca^{2+}$  transient due to photobleaching. The limit of resolution of  $V_{1/2}$ , the parameter with the largest error, was estimated with a z-test which formally tests for the difference between the mean of a population and a hypothetical mean. We determined the smallest difference between an experimental and a hypothesized  $V_{1/2}$  resolvable at a level of statistical confidence  $p < 0.05$ . In the calculations, we used the data with the largest  $V_{1/2}$  variance for each measurement (conductance, charge movement and fluorescence). Also, we assumed a hypothetical S.D. equal to the experimental S.D. The estimated limits of statistical resolution were  $\sim 3.9$  mV for conductance,  $\sim 6.5$  mV for charge movements, and  $\sim 8.5$  mV for fluorescence measurements. Thus, a difference in population mean  $V_{1/2}$  of less than the indicated limit would not be statistically significant, given the variance and the number of determinations of the present study. Statistical analyses were performed with Analyse-it software (Leeds, UK)

### List of Abbreviations

AID ( $\alpha$  subunit interaction domain); BID ( $\beta$  subunit interaction domain); DMSO (dimethyl sulfoxide); EGTA (ethylene glycol bis-aminoethylether tetraacetic acid); HEPES (2-hydroxyethyl piperazine 2-ethane sulfonic acid); MOPS (3N-Morpholino-propane sulfonic acid); PVDF (polyvinylidene difluoride); TTX (tetrodotoxin); TEA (tetraethylammonium).

### Acknowledgements

Supported by National Institutes of Health Grant HL-47053 (R.C., P.A.P., and R.G.G.), AR46448 (R.C.), National Science Foundation IBN-9319540 (R.G.G. and P.A.P.) and by a predoctoral fellowship from Wisconsin Heart Association (C.A.A.). K.P.C. is an investigator of the Howard Hughes Medical Institute.

### References

- Perez-Reyes E, Schneider T: **Calcium channels: Structure, Function, and Classification.** *Drug Dev Res* 1994, **33**:295-318
- McPherson PS, Campbell KP: **The ryanodine receptor/ $Ca^{2+}$  release channel.** *J Biol Chem* 1993, **268**:13765-13768
- Rios E, Pizarro G: **Voltage sensor of excitation-contraction coupling in skeletal muscle.** *Physiol Revs* 1991, **71**:849-908
- Tanabe T, Beam KG, Adams BA, Niidome T, Numa S: **Regions of the skeletal muscle dihydropyridine receptor critical for excitation-contraction coupling.** *Nature* 1990, **346**:567-572
- Nakai J, Tanabe T, Konno T, Adams B, Beam KG: **Localization in the II-III loop of the dihydropyridine receptor of a sequence critical for excitation-contraction coupling.** *J Biol Chem* 1998, **273**:24983-24986
- Pragnell M, DeWaard M, Mori Y, Tanabe T, Snutch TP, Campbell KP: **Calcium channel  $\beta$ -subunit binds to a conserved motif in the I-II cytoplasmic linker of the  $\alpha 1$ -subunit.** *Nature* 1994, **368**:67-70
- De Waard M, Pragnell M, Campbell KP:  **$Ca^{2+}$  channel regulation by a conserved  $\beta$  subunit domain.** *Neuron* 1994, **13**:495-503
- Birnbaumer L, Qin N, Olcese R, Tareilus E, Platano D, Costantin D, Stefani E: **Structures and functions of calcium channel  $\beta$  subunits.** *J Bioenerg Biomemb* 1998, **30**:357-375
- Gurnett CA, Campbell KP: **Transmembrane auxiliary subunits of voltage-dependent ion channels.** *J Biol Chem* 1996, **271**:27975-27978
- Gurnett CA, De Waard M, Campbell KP: **Dual function of the voltage-dependent  $Ca^{2+}$  channel  $\alpha 2$ - $\delta$  subunit in current stimulation and subunit interaction.** *Neuron* 1996, **16**:431-440
- Sharp AH, Campbell KP: **Characterization of the 1,4 dihydropyridine receptor using subunit-specific polyclonal antibodies: evidence of a 32,000-Da subunit.** *J Biol Chem* 1989, **264**:2816-2825
- Jay SD, Ellis SB, McCue AF, Williams ME, Vedvick TS, Harpold MM, Campbell KP: **Primary structure of the  $\gamma$  subunit of the L-type calcium channel from rabbit skeletal muscle.** *Science* 1990, **248**:490-492
- Bosse E, Regulla S, Biel M, Ruth P, Meyer HE, Flockerzi V, Hofmann F: **The cDNA and deduced amino acid sequence of the  $\gamma$  subunit of the L-type calcium channel from rabbit skeletal muscle.** *FEBS Letters* 1990, **267**:153-156
- Gregg RG, Messing A, Strube C, Beurq M, Moss R, Behan M, Sukhareva M, Haynes S, Powell JA, Coronado R, Powers PA: **Absence of the  $\beta$  subunit (cchb1) of the skeletal muscle dihydropyridine receptor alters expression of the  $\alpha 1$  subunit and eliminates excitation-contraction coupling.** *Proc Natl Acad Sci USA* 1996, **93**:13961-13966
- Beurq M, Ahern CA, Vallejo P, Conklin MW, Powers PA, Gregg RG, Coronado R: **Involvement of the carboxy-terminus region of the dihydropyridine receptor  $\beta 1a$  subunit in excitation-contraction coupling of skeletal muscle.** *Biophys J* 1999, **77**:2953-2967
- Qin N, Olcese R, Stefani E, Birnbaumer L: **Modulation of human neuronal  $\alpha 1E$ -type calcium channel by  $\alpha 2$ - $\delta$  subunit.** *Am J Physiol* 1998, **274**:C1324-C1331
- Letts VA, Felix R, Biddlecome GH, Arikkath J, Mahaffey CL, Valenzuela A, Bartlett FS, Mori Y, Campbell KP, Frankel WN: **The mouse stargazer gene encodes a neuronal  $Ca^{2+}$  channel  $\gamma$  subunit.** *Nature Genet* 1998, **19**:340-347
- Klugbauer N, Dai S, Specht V, Lacinova L, Marais E, Bohn G, Hofmann F: **A family of  $\gamma$ -like calcium channel subunits.** *FEBS Lett* 2000, **470**:189-197
- Burgess DL, Gefrides LA, Foreman PJ, Noebels JL: **A cluster of three novel  $Ca^{2+}$  channel  $\gamma$  subunit genes in chromosome 19q13.4: Evolution and expression profile of the  $\gamma$  subunit family.** *Genomics* 2001, **71**:339-350
- Freise D, Held B, Wissenbach U, Pfeifer A, Trost C, Himmerkus N, Schweig U, Freichel M, Biel M, Hofmann F, Hoth M, Flockerzi V: **In-**

- activation properties and current densities of skeletal muscle L-type calcium channel are altered in  $\gamma 1$  deficient mice. *J Biol Chem* 2000, **275**:14476-14481
21. Morrill JA, Brown RH Jr, Cannon SC: **Gating of the L-type  $\text{Ca}^{2+}$  channel in human skeletal myotubes: An activation defect caused by the hypokalemic periodic paralysis mutation R528H.** *J Neurosci* 1998, **18**:10320-10334
  22. Sipos I, Pika-Hartlaub U, Hofmann F, Flucher BE, Melzer W: **Effects of the dihydropyridine receptor subunits gamma and alpha2delta on the kinetics of heterologously expressed L-type  $\text{Ca}^{2+}$  channels.** *Pflugers Arch* 2000, **439**:691-699
  23. Singer D, Biel M, Lotan I, Flockerzi V, Hofmann F, Dascal N: **The roles of the subunits in the function of the calcium channel.** *Science* 1991, **253**:1553-1557
  24. Wei X, Perez-Reyes E, Lacerda AE, Schuster G, Brown AM, Birnbaumer L: **Heterologous regulation of the cardiac  $\text{Ca}^{2+}$  channel  $\alpha 1$  subunit by skeletal muscle  $\beta$  and  $\gamma$  subunits.** *J Biol Chem* 1991, **266**:21943-21947
  25. Lerche H, Klugbauer N, Lehmann-Horn F, Hofmann F, Melzer W: **Expression and functional characterization of the cardiac L-type calcium channel carrying a skeletal muscle DHP receptor mutation causing hypokalaemic periodic paralysis.** *Pflugers Arch* 1996, **431**:461-463
  26. Eberst R, Dai S, Klugbauer N, Hofmann F: **Identification and functional characterization of a calcium channel  $\gamma$  subunit.** *Pflugers Arch* 1987, **433**:633-637
  27. Garcia J, Beam KG: **Relationship of calcium transients to calcium currents and charge movements in myotubes expressing skeletal and cardiac dihydropyridine receptors.** *J Gen Physiol* 1994, **103**:125-147
  28. Ahern CA, Arikath J, Vallejo P, Gurnett CA, Powers PA, Campbell KP, Coronado R: **Intramembrane charge movements and excitation-contraction coupling expressed by two-domain fragments of the  $\text{Ca}^{2+}$  channel.** *Proc Natl Acad Sci USA* 2001, **98**:6935-6940
  29. Strube C, Beurg M, Powers PA, Gregg RG, Coronado R: **Reduced  $\text{Ca}^{2+}$  current, charge movement and absence of  $\text{Ca}^{2+}$  transients in skeletal muscle deficient in dihydropyridine receptor** *Biophys J* 1996, **71**:2531-2543
  30. Beurg M, Sukhareva M, Ahern CA, Conklin MW, Perez-Reyes E, Powers PA, Gregg RG, Coronado R: **Differential control of skeletal muscle  $\text{Ca}^{2+}$  current and excitation-contraction coupling by the dihydropyridine receptor  $\beta$  subunit.** *Biophys J* 1999, **76**:1744-1756
  31. Melzer W, Schneider MF, Simon BJ, Szucs G: **Intramembrane charge movement and calcium release in frog skeletal muscle.** *J Physiol (Lond)* 1986, **373**:481-511
  32. Ursu D, Sebillé S, Dietze B, Freise D, Flockerzi V, Melzer W: **Excitation-contraction coupling in skeletal muscle of a transgenic mouse lacking the dihydropyridine receptor subunit gamma1.** *J Physiol (Lond)* 2001, **533**:367-377
  33. Shirokov R, Ferreira G, Yi J, Rios E: **Inactivation of gating currents of L-type calcium channels. Specific role of the  $\alpha 2\delta$  subunit.** *J Gen Physiol* 1998, **111**:807-823
  34. Neely A, Wei X, Olcese R, Birnbaumer L, Stefani E: **Potentiality by the  $\beta$  subunit of the ratio of the ionic current to the charge movement in the cardiac calcium channel.** *Science* 1993, **262**:575-578
  35. Neely A, Olcese R, Baldelli P, Wei X, Birnbaumer L, Stefani E: **Dual activation of the cardiac  $\text{Ca}^{2+}$  channel IC-subunit and its modulation by the  $\beta$ -subunit.** *Am J Physiol Cell Physiol* 1995, **268**:C732-C740
  36. Olcese R, Qin N, Schneider T, Neely A, Wei X, Stefani E, Birnbaumer L: **The amino terminus of a calcium channel  $\beta$  subunit sets rates of channel inactivation independently of the subunit's effect on activation.** *Neuron* 1994, **13**:1433-1438
  37. Qin N, Olcese R, Zhou JM, Cabello OA, Birnbaumer L, Stefani LE: **Identification of a second region of the  $\beta$ -subunit involved in regulation of calcium channel inactivation.** *Am J Physiol Cell Physiol* 1996, **271**:C1539-C1545
  38. Nakai J, Sekiguchi N, Rando TA, Allen PD, Beam KG: **Two regions of the ryanodine receptor involved in coupling with L-type  $\text{Ca}^{2+}$  channels.** *J Biol Chem* 1998, **273**:13403-13406
  39. Dirksen RT, Beam KG: **Role of calcium permeation in dihydropyridine receptor function. Insights into channel gating and excitation-contraction coupling.** *J Gen Physiol* 1999, **114**:393-403
  40. Schneider MF, Chandler WK: **Voltage-dependent charge movement in skeletal muscle: a possible step in excitation-contraction coupling.** *Nature* 1973, **242**:244-246
  41. Ramirez-Solis R, Davis AC, Bradley A: **Gene targeting in embryonic stem cells.** *Methods Enzymol* 1993, **225**:855-878
  42. Witcher DR, De Waard M, Kahl SD, Campbell KP: **Purification and reconstitution of the N-type calcium channel complex from rabbit brain.** *Methods Enzymol* 1994, **238**:335-348
  43. Leung AT, Imagawa T, Campbell KP: **Structural characterization of the I,4 dihydropyridine receptor of the voltage-dependent  $\text{Ca}^{2+}$  channel from rabbit skeletal muscle: evidence for two distinct high molecular weight subunits.** *J Biol Chem* 1987, **262**:7943-7946
  44. Pragnell M, Sakamoto J, Jay SD, Campbell KP: **Cloning and tissue-specific expression of the brain calcium channel  $\beta$ -subunit.** *FEBS Lett.* 1991, **291**:253-258
  45. Beurg M, Sukhareva M, Strube C, Powers PA, Gregg RG, Coronado R: **Recovery of  $\text{Ca}^{2+}$  current, charge movements, and  $\text{Ca}^{2+}$  transients in myotubes deficient in dihydropyridine receptor  $\beta 1$  subunit transfected with  $\beta 1$  cDNA.** *Biophys J* 1997, **73**:807-818
  46. Conklin MW, Ahern CA, Vallejo P, Sorrentino V, Takeshima H, Coronado R: **Comparison of  $\text{Ca}^{2+}$  sparks produced independently by two ryanodine receptor isoforms (type-1 or type-3).** *Biophys J* 2000, **78**:1777-1785
  47. Conklin MW, Barone V, Sorrentino V, Coronado R: **Contribution of ryanodine receptor type-3 to  $\text{Ca}^{2+}$  sparks in embryonic mouse skeletal muscle.** *Biophys J* 1999, **77**:1394-1403
  48. Conklin MW, Powers PA, Gregg RG, Coronado R:  **$\text{Ca}^{2+}$  sparks in embryonic mouse skeletal muscle selectively deficient in dihydropyridine receptor  $\alpha 1S$  or  $\beta 1$  subunits.** *Biophys J* 1999, **76**:657-669

Publish with **BioMedcentral** and every scientist can read your work free of charge

"BioMedcentral will be the most significant development for disseminating the results of biomedical research in our lifetime."

Paul Nurse, Director-General, Imperial Cancer Research Fund

Publish with **BMC** and your research papers will be:

- available free of charge to the entire biomedical community
- peer reviewed and published immediately upon acceptance
- cited in PubMed and archived on PubMed Central
- yours - you keep the copyright



Submit your manuscript here:

<http://www.biomedcentral.com/manuscript/>

[editorial@biomedcentral.com](mailto:editorial@biomedcentral.com)